Chinese Chemical Letters 37 (2026) 111640

Contents lists available at ScienceDirect

Chinese Chemical Letters

journal homepage: www.elsevier.com/locate/cclet

Enhanced tetracycline degradation *via* nano zero-valent iron confined in halloysite nanotubes for sustainable water purification

Yi Zhou[a], Guocheng Lv[a,*], Xinyu Lei[a], Xinyu Hou[a], Meng Liu[a], Libing Liao[a], Hailiang Dong[b,*]

[a] Engineering Research Center of Ministry of Education for Geological Carbon Storage and Low Carbon Utilization of Resources, Beijing Key Laboratory of Materials Utilization of Nonmetallic Minerals and Solid Wastes, National Laboratory of Mineral Materials, Hebei Key Laboratory of Resource Low-carbon Utilization and New Materials, School of Materials Science and Technology, China University of Geosciences (Beijing), Beijing 100083, China
[b] Center for Geomicrobiology and Biogeochemistry Research, State Key Laboratory of Biogeology and Environmental Geology, China University of Geosciences, Beijing 100083, China

ARTICLE INFO

Article history:
Received 19 June 2025
Revised 14 July 2025
Accepted 25 July 2025
Available online 30 July 2025

Keywords:
Nanoscale zero-valent iron
Halloysite nanotubes
Confined space
Fenton-like reaction
Contaminant degradation

ABSTRACT

Environmental remediation demands efficient strategies for antibiotic degradation. Herein, we report the successful selective loading of nano zero-valent iron (nZVI) into the lumen of halloysite nanotubes (HNTs) *via* vacuum-assisted infusion and thermal reduction (denoted as nZVI@HNTs). This confined nanoreactor architecture simultaneously acts as a robust reductant and a Fenton-like catalyst. The tubular structure of HNTs enhanced nZVI dispersion and stability while leveraging its nanoconfinement effect to concentrate pollutants and suppress parasitic reactions between nZVI and H_2O_2. For tetracycline (TC) degradation, the nZVI@HNTs + H_2O_2 system achieved 86.61 % removal within 90 min (20 mg/L TC, pH 5.5), outperforming surface-loaded controls by >19 %. Crucially, the HNT lumen provides dual protection: Spatial isolation suppresses non-target nZVI consumption by O_2/H_2O, while constrained diffusion delays H_2O_2 contact, prioritizing contaminant reduction before controlled Fe^{2+}-activated oxidation. Reactive oxygen species (ROS), including ·OH, $\cdot O_2^-$, and $^1O_2$, synergistically drove TC degradation through radical and nonradical pathways. LC-MS analysis identified intermediates formed *via* demethylation, ring opening, and hydroxylation, with toxicity assessments confirming reduced acute toxicity, mutagenicity, and developmental toxicity of byproducts. Notably, nZVI@HNTs retained 64.03 % efficiency after five cycles, demonstrating superior reusability. This work provides a novel strategy to enhance nZVI's environmental applicability by combining confinement engineering with redox-coupled processes, offering broad prospects for sustainable water purification.

© 2026 Published by Elsevier B.V. on behalf of Chinese Chemical Society and Institute of Materia Medica, Chinese Academy of Medical Sciences.

The persistent global challenge of water pollution from inadequately removed recalcitrant contaminants, which threatens human health and aquatic ecosystems, makes developing efficient and economical water purification technologies imperative [1,2]. Nanoscale zero-valent iron (nZVI) has been utilized for pollutant treatment for several decades due to its strong reducing ability, efficient electron transfer capacity, and relatively non-toxicity [3–5]. As a versatile reductant, nZVI effectively eliminates contaminants that readily accept electrons, including halogenated organic compounds, antibiotics, dyes, nitrates, and heavy metals [6–8]. However, nZVI's degradation rate and efficiency lag behind those of advanced oxidation processes (AOPs) [9,10]. Importantly, the release of Fe^{2+} through the interaction of nZVI with organic pollutants can activate hydrogen peroxide (H_2O_2), initiating the Fenton-like process (Eqs. 1 and 2) [11,12].

$$\text{contaminant} + \text{nFe}^0 + \text{nH}^+ \rightarrow \text{reactionintermediates} + \text{CO}_2 \uparrow + \text{H}_2\text{O} + \text{nFe}^{2+} \quad (1)$$

$$\text{Fe}^{2+} + \text{H}_2\text{O}_2 \rightarrow \text{Fe}^{3+} + \cdot\text{OH} + \text{OH}^- \quad (2)$$

The Fenton-like reaction is widely recognized among AOPs for the generation of highly reactive oxygen species (ROS), which effectively degrade a wide range of organic pollutants [13,14]. Combining nZVI reduction with the Fenton oxidation (nZVI-Fenton) process enhances contaminant removal significantly. Li *et al.* demonstrated that the nZVI-Fenton process achieves more effective removal of *p*-chloronitrobenzene (*p*-ClNB) from groundwater

* Corresponding authors.
E-mail addresses: guochenglv@cugb.edu.cn (G. Lv), dongh@cugb.edu.cn (H. Dong).

https://doi.org/10.1016/j.cclet.2025.111640
1001-8417/© 2026 Published by Elsevier B.V. on behalf of Chinese Chemical Society and Institute of Materia Medica, Chinese Academy of Medical Sciences.

compared to either nZVI or Fenton reaction alone [15]. Additionally, nZVI acts as a reactive heterogeneous catalyst, gradually releasing Fe^{2+} and addressing drawbacks of the traditional Fenton reaction, such as rapid Fe^{2+} depletion and increased sludge production [16,17].

However, several challenges persist in this collaborative process. Firstly, due to its inherent magnetism and high surface energy, nZVI often exhibits limited dispersibility in sewage, which reduces the mass-transfer benefits of its large specific surface area [18,19]. By anchoring nZVI onto suitable carriers can mitigate this issue [20]. For example, Hussain *et al*. enhanced the degradation efficiency of nonylphenol by nearly 2.5 times by immobilizing nZVI onto biochar [21]. Carriers stabilize nZVI distribution and increase its contact opportunities with contaminants due to their high adsorption capacity. Secondly, nZVI is susceptible to consumption by H_2O, O_2, H^+, and H_2O_2 (Eqs. 3-7), posing challenges in preserving nZVI and shortening its operational lifespan [22]. It is crucial to implement protective measures against nonspecific reactions. For example, Li *et al.* demonstrated that coating nZVI with a $Mg(OH)_2$ shell significantly reduces water-induced corrosion and controls Fe^{2+} dissolution [23]. Tang *et al*. found that carbon coatings effectively inhibit nZVI agglomeration and extend its storage stability in air for over 120 days [24].

$$Fe^0 + 2H_2O \rightarrow Fe^{2+} + H_2 \uparrow + 2OH^- \quad (3)$$

$$2Fe^0 + 4H^+ + O_2 \rightarrow 2Fe^{2+} + 2H_2O \quad (4)$$

$$Fe^0 + 2H^+ \rightarrow Fe^{2+} + H_2 \uparrow \quad (5)$$

$$2Fe^0 + O_2 + H_2O \rightarrow 2Fe^{2+} + 4OH^- \quad (6)$$

$$Fe^0 + 2H_2O_2 + 2H^+ \rightarrow Fe^{2+} + 2H_2O \quad (7)$$

Thus, loading nZVI into confined spaces (metal-organic framework materials (MOFs) [25], 2D membranes [26], clay minerals [27], carbon nanotubes (CNTs) [28], *etc.*) holds promise as a solution to these challenges. Halloysite nanotubes (HNTs, $Al_2Si_2O_5(OH)_4{\cdot}nH_2O$, n = 0 or 2), found in natural clay minerals, exhibits the potential to integrate the aforementioned advantages of multiple materials. It features abundant reserves and unique tubular structure [29,30]. Moreover, HNTs offer large specific surface areas, chemical durability, and practical advantages [31,32]. Unlike synthetic CNTs/MOFs requiring complex functionalization, raw HNTs enable vacuum-driven encapsulation at ambient conditions. Some studies have shown that Au, Pd, and CeO_2 can be selectively loaded into HNT lumen, and their long-term stability in wound healing, catalysis, and UV protection increases [33–35]. However, highly efficient and selective loading of nZVI within the interior lumen of HNTs remains scarcely reported, particularly for applications involving Fenton-like reaction activation to degrade organic contaminants.

Hence, this study involved the selective loading of nZVI into HNT lumens (nZVI@HNTs) using a combination of vacuum loading and heat reduction treatment (Fig. S1 in Supporting information). nZVI@HNTs serve dual roles as effective reducers of organic pollutants and activators of H_2O_2. As the world's most prevalent antibiotics, tetracycline (TC) was chosen as the target pollutant to systematically investigate influencing factors and the reaction mechanism, as well as determining optimal conditions. The study also explored the relationship between the long-term stability of nZVI@HNTs and structural effects of this composite material. Crucial reactive species were identified through radical scavenging experiments and electron spin resonance (ESR) spectroscopy. Finally, potential degradation pathways were analyzed, and the overall toxicity of intermediates was assessed using the Toxicity Estimation Software Tool (T.E.S.T.) based on quantitative structure-activity relationship (QSAR) predictions. This research offers a novel perspective on enhancing the application nZVI in environmental remediation.

Chemicals are listed in Text S1 (Supporting information). The synthesis details of nZVI loaded in the HNT lumen (nZVI@HNTs), nZVI loaded on the external surface of HNTs (nZVI/HNTs), and nZVI nanoparticles (nZVI NPs) are described in Text S2 (Supporting information). The details of Characterizations are provided in Text S3 (Supporting information).

All degradation experiments were conducted in darkness at a controlled temperature of 20 ±2 °C. Initially, 50 mg of nZVI@HNTs was added to 100 mL of TC aqueous solution (20 mg/L). After stirring for 30 min, 60 μL of H_2O_2 was introduced into the suspension. Samples of 4 mL were withdrawn at specific intervals and promptly mixed with 4 mL of MeOH to halt the reaction. The absorbance of these filtered samples, passed through a 0.22 μm filter membrane, was then measured at the maximum absorption wavelength of 357 nm using a UV–vis spectrophotometer (UV-2600, Shimadzu).

The degradation of TC in the presence of nZVI@HNTs was examined by varying several factors: The dosage of nZVI@HNTs, the amount of H_2O_2, the concentration of the TC solution, the pH of the TC solution, the dissolved oxygen (DO) concentration, and the inorganic anions effects. Furthermore, the types of reactive species and their impacts were investigated by introducing free radical scavengers (MeOH, *p*-BQ, and L-histidine). MeOH, *p*-BQ, and L-histidine were used to limit the reactivity of $OH\cdot$, $\cdot O_2^-$, and $^1O_2$ with contaminants, respectively, due to their different reaction capacity with ROS (the second-order rate constants listed in Table S1 in Supporting information). To assess the cycle life of nZVI@HNTs, nZVI/HNTs, and nZVI, materials recovered from the reaction system were subjected to 5 reaction cycles under identical conditions.

XRD analysis (Fig. 1a) confirmed the crystalline structure and phase composition of nZVI@HNTs. The peaks observed at $2\theta = 44.7°$ (110), 65.0° (200), and 82.3° (211) in the XRD pattern matched the characteristic reflections in the standard pattern (JCPDS No. 06–0696), indicating successful synthesis of nZVI [36]. No additional peaks were detected, confirming the purity of the synthesized nZVI. Furthermore, compared to the XRD pattern of

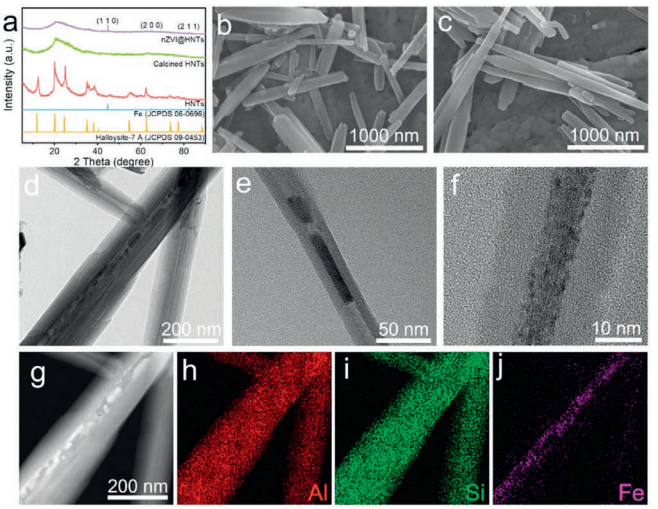


Fig. 1. (a) XRD patterns of nZVI@HNTs, calcined HNTs, and HNTs. (b, c) SEM images of nZVI@HNTs. (d, e) TEM images of nZVI@HNTs. (f) High-resolution TEM image of the nZVI@HNTs. (g) HADDF-STEM image of the nZVI@HNTs. (h-j) Elemental distribution (EDX mapping) of the nZVI@HNTs: Al, Si, and Fe.

pristine HNTs, the pattern of nZVI@HNTs showed a reduction in the intensity of HNTs peaks. This change was influenced not by the presence of nZVI but by the heat-reduction treatment, which altered the crystalline structure of HNTs. The TGA profile shows that structural water in the HNTs is primarily lost as temperatures increase beyond 500 °C (Fig. S2 in Supporting information), which leads to collapse of the octahedral layer and a consequent weakening of the corresponding peak intensity [37]. However, the tubular structure of the HNTs did not shrink or collapse after heat reduction according to the SEM and TEM images (Fig. S3 in Supporting information) of HNTs and calcined HNTs. The HNTs used had an average inner diameter of 17.58 nm and an average outer diameter of 71.31 nm. The length of the HNTs was about 0.2-3 μm. In addition, XPS analysis further investigated the valence state of iron. The wide-scan XPS spectrum of nZVI@HNTs shows peaks at 712.0, 532.8, 103.7, and 75.7 eV corresponding to Fe 2p, O 1s, Si 2p, and Al 2p, respectively (Fig. S4a in Supporting information). Fe 2p spectra can be deconvoluted into four typical peaks for Fe^{2+} $2p_{1/2}$ (725.01 eV), Fe^{2+} $2p_{3/2}$ (711.5 eV), Fe^{3+} $2p_{1/2}$ (731.22 eV), and Fe^{3+} $2p_{3/2}$ (716.96 eV) (Fig. S4b in Supporting information) [38,39]. Notably, peaks characteristic of Fe^0 at 706.9 and 719.9 eV are absent. This suggests potential oxidation of nZVI on the edge of HNTs or that nZVI within HNTs may not be detectable by XPS [24,40]. Furthermore, nZVI@HNTs exhibited negligible mass loss before reaching 900 °C (Fig. S2 in Supporting information), indicating the absence of iron oxides [41].

The external surface of nZVI@HNTs appeared smooth with almost no attached nanoparticles (Figs. 1b and c), indicating that nZVI did not grow on the outside surface of the HNTs. TEM images showed nZVI dispersed within the lumen of the HNTs (Figs. 1d and e), with particle sizes generally equal to or smaller than the inner diameter of the HNTs. High-resolution TEM image (Fig. 1f) revealed that nZVI particles aggregated from smaller particles, about 2 nm in size. Additionally, elemental distribution maps indicated that Fe was more concentrated within the lumen compared to Al and Si (Figs. 1g-j and Fig. S5 in Supporting information). The hollow structure of HNTs provided a confined nanoscale space with higher vapor pressure, promoting faster solvent evaporation [42]. This pressure differential facilitated continuous solution transfer into the nanotubes, enhancing the enrichment of guest molecules within HNTs. Fe^{3+} ions remaining on the outer surface of HNTs could be easily removed by washing due to strong electrostatic repulsion under acidic conditions. The surface area and average pore diameter of nZVI@HNTs were analyzed using N_2 adsorption-desorption isotherms (Fig. S6 and Table S2 in Supporting information). Both HNTs and nZVI@HNTs exhibited type IV isotherms with an H3 hysteresis loop, characteristic of long and narrow channels provided by HNTs [43]. Compared to pristine HNTs, the BET surface area and average pore diameter of nZVI@HNTs were slightly reduced (23.35 m^2/g and 12.93 nm *vs.* 24.27 m^2/g and 18.75 nm for HNTs), reflecting the partial filling of the HNT lumens by nZVI. ICP-OES determined about 8.75 % nZVI content in nZVI@HNTs (Table S3 in Supporting information). Furthermore, the saturation magnetization values of nZVI@HNTs and nZVI NPs were 3.09 and 41.03 emu/g, respectively (Fig. S7 in Supporting information). The lower mass ratio of nZVI within nZVI@HNTs contributed to the reduced saturation magnetization, which minimized agglomeration and aggregation tendencies.

The removal efficiency of 20 mg/L TC over 90 min under different conditions was compared to investigate the degradation mechanism of nZVI@HNTs + H_2O_2 (Fig. 2a). Initially, TC removal was minimal with H_2O_2 addition only, indicating no significant interaction between H_2O_2 and TC without catalysts. The TC removal efficiencies of HNTs and HNTs + H_2O_2 were 19.03 % and 17.62 %, respectively, highlighting that H_2O_2 activation by HNTs was ineffective, and TC removal primarily relied on HNTs adsorption [44,45]. The degradation process was analyzed in three stages: Stage 1 involved only the catalyst for the first 30 min, stage 2 began immediately after adding H_2O_2, and stage 3 spanned 5-60 min post H_2O_2 addition. The degradation rates for each stage, denoted as k_1, k_2, and k_3, were calculated (Fig. 2b). During stage 1, HNT adsorption reached equilibrium, with a *pseudo*-first-order kinetic constant of 0.0063 min^{-1}, indicating effective concentration of low-concentration pollutants by adsorption [46].

The TC removal efficiency achieved by nZVI@HNTs + H_2O_2 was notably higher at about 86.61 %, compared to 67.10 % with nZVI@HNTs alone. In stage 1, the degradation capability of nZVI@HNTs against TC was facilitated by both HNT adsorption and nZVI reduction. TC molecules were adsorbed into the HNT lumens and came into contact with nZVI loaded on the inner surface of the HNTs, initiating TC degradation. As TC underwent reduction, Fe^{2+} ions were released, capable of activating H_2O_2 to generate ROS. Fe^{2+} release tests from nZVI@HNTs indicated higher iron ion release in the presence of 20 mg/L TC (33.7 μg/L) compared to DI water (7.9 μg/L), confirming the strong reactivity between nZVI@HNTs and TC (Fig. S8a in Supporting information). Consequently, TC degradation efficiency rapidly improved to 82.74 % in stage 2. The degradation rate was notably accelerated by the nZVI-Fenton process, with k_2 (0.2240 min^{-1}) about twice as fast as k_1 (0.0212 min^{-1}). The timing of H_2O_2 introduction was crucial (Fig. S8b in Supporting information): Simultaneous addition of nZVI@HNTs and H_2O_2 resulted in a 11.69 % lower TC degradation efficiency compared to sequential addition after 30 min, and this difference increased to 39.02 % within the first 35 min. This was attributed to initial H_2O_2 addition leading to surface passivation and oxidation of nZVI, mutually consuming nZVI and H_2O_2 and hindering both TC reduction and ROS generation. In contrast, such passivation effect was minimal with sequential addition of H_2O_2. Therefore, the stepwise combination of nZVI@HNT reduction and Fenton oxidation processes optimizes the utilization of nZVI and H_2O_2 for efficient TC degradation.

The impact of nZVI@HNT dosage ranging from 0.05 g/L to 1 g/L was examined (Fig. 2c). In stage 1, as the nZVI@HNT dose increased, both the removal efficiency and rates (Fig. S9a in Supporting information) of TC showed proportional enhancement. This outcome stemmed from increased nZVI participation in TC degradation, facilitated by greater availability of surface and active sites, resulting in higher Fe^{2+} concentrations in the solution for H_2O_2 activation [47]. Moreover, in stage 2, TC degradation rates progressively rose with increasing nZVI@HNT doses from 0.05 g/L ($k_2 = 0.0172$ min^{-1}) to 0.5 g/L ($k_2 = 0.2240$ min^{-1}). However, with further increases to 1 g/L ($k_2 = 0.0915$ min^{-1}), TC degradation rates declined. This phenomenon may be attributed to (1) lower residual TC concentrations reducing reaction collisions and (2) approaching saturation of free Fe^{2+} availability for H_2O_2 activation when using 0.5 g/L nZVI@HNTs. Considering cost-effectiveness, 0.5 g/L of nZVI@HNTs was selected for all subsequent experiments.

As a major and direct source of ROS, H_2O_2 plays a pivotal role in TC degradation. The impact of H_2O_2 concentration (0–0.79 mmol/L) was investigated (Fig. 2d). At 0.49 mmol/L H_2O_2, TC degradation efficiency was only 75.35 %, gradually improving with higher H_2O_2 concentrations. Additionally, k_2 increased with rising H_2O_2 level (Fig. S9b in Supporting information), as more activated H_2O_2 led to increased ROS production. The optimal H_2O_2 concentration for TC degradation was found to be 5.87 mmol/L, maintaining TC degradation efficiency stable at about 86.61 %. Several factors contribute to this observation: initially, Fe^{2+} released in the first 30 min cannot activate additional H_2O_2. Excessive H_2O_2 can also occupy active sites on nZVI@HNTs, hindering Fe^{2+} release. Moreover, surplus H_2O_2 reacts with ·OH to form $\cdot O_2^-$ or $\cdot HO_2^-$·

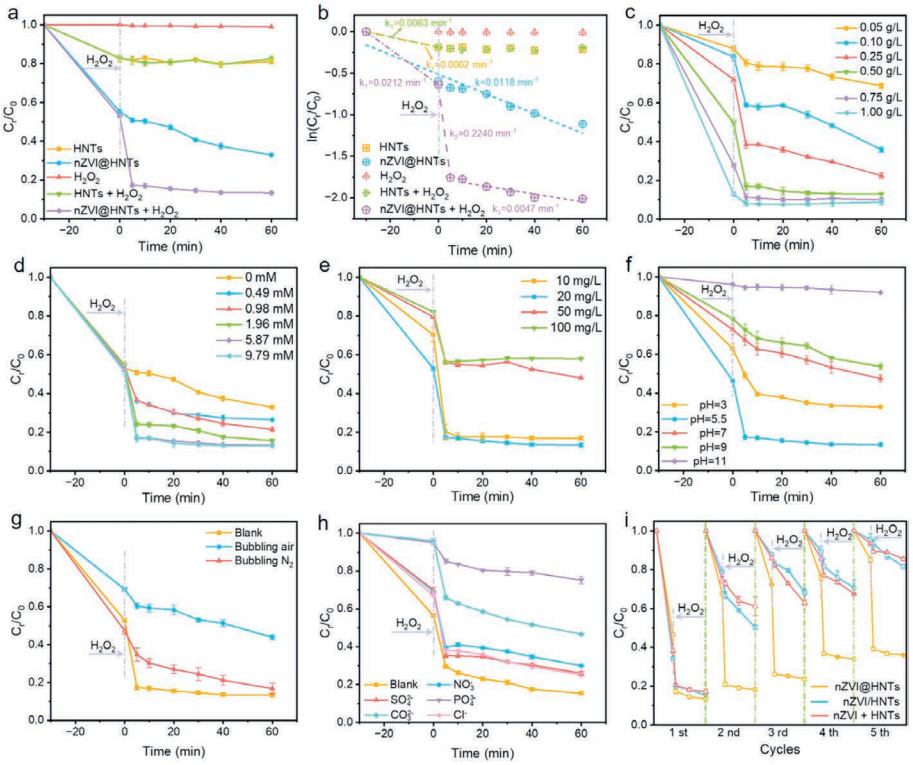


Fig. 2. (a) TC removal performance and (b) corresponding *pseudo*-first-order degradation kinetic plots for the different systems (Reaction conditions: [TC] = 20 mg/L, initial pH 5.5, catalyst dosage = 0.5 g/L, and H_2O_2 concentration = 5.87 mmol/L). (c) Influence of catalyst dose, (d) H_2O_2 concentration, (e) TC concentration, (f) initial pH, (g) DO and (h) inorganic anions on TC degradation. (i) Comparison of the TC removal performances of nZVI@HNTs, nZVI/HNTs, and the physical mixture of nZVI and HNTs after 5 cycles.

(Eq. 8) [48]. The scavenging effect of ·OH limits the enhancement of TC degradation efficiency with increasing H_2O_2 concentration.

$$\cdot OH + H_2O_2 \rightarrow \cdot O_2^- / \cdot HO_2^- + H_2O \quad (8)$$

Fig. 2e demonstrates how the initial concentration of TC influences its degradation efficiency. Lower concentrations of TC (10 mg/L: 83.11 % and 20 mg/L: 86.61 %) exhibited significantly higher degradation efficiencies compared to higher concentrations (50 mg/L: 52.00 % and 100 mg/L: 41.97 %). This trend arises because at lower TC concentrations, there is a more favorable molar ratio of nZVI@HNTs to TC, enabling more effective action of nZVI and ROS per TC molecule, thereby enhancing degradation. Interestingly, both the degradation efficiency and rates (Fig. S9c in Supporting information) of 20 mg/L TC (47.10 % and 0.0212 min^{-1}) exceeded those of 10 mg/L TC (29.73 % and 0.0118 min^{-1}) during stage 1. This was attributed to the higher concentration accelerating the occupation of adsorption sites on nZVI@HNTs by TC molecules [49]. However, this trend was reversed upon the addition of H_2O_2 to initiate AOPs, where ROS effectively removed TC more rapidly at lower initial concentrations.

During the process of organic degradation, the efficiency of both nZVI and the Fenton reaction is highly influenced by the pH level of the solution [50]. The performance of nZVI@HNTs under different pH conditions (ranging from pH 3 to pH 11) was compared (Fig. 2f and Fig. S9d in Supporting information). Notably, the removal efficiency of TC was significantly higher at pH 5.5 compared to other initial pH values. This difference stems from distinct degradation mechanisms operating at different stages of the reaction. Initially, when nZVI@HNTs are introduced into the TC solution, adsorption plays a pivotal role. The adsorption capacity is determined by the surface charge of nZVI@HNTs and the ionized forms of TC, both of which vary with the solution pH. The surface charge of nZVI@HNTs at different pH levels (Table S4 in Supporting information) correlates with the point of zero charge (PZC) of the inner and outer surfaces of HNTs, as well as the nZVI itself (8.5, 1.75, and 7.3, respectively) [51,52]. The distribution of ionogenic group states (Fig. S10 in Supporting information) and the net charge of TC (Table S5 in Supporting information) were calculated based on its pK_a values (pK_{a1}=3.4 ± 0.4 and pK_{a2}=9.4 ± 0.4). Therefore, the closer the solution pH approaches neutral, the more favorable adsorption becomes, primarily driven by electrostatic interactions. However, the reaction between nZVI in HNTs and TC is more adaptable to acidic environments. An abundance of H^+ prevents the formation of a passivation film and promotes a shift in the reaction balance toward pollutant degradation [38]. Therefore, the optimal degradation efficiency (50.00 %) and rate (0.0212 min^{-1}) were observed at pH 5.5 during stage 1. As more TC is consumed, higher amounts of iron ions are generated, which enhances the degradation rate during stage 2. Thus, pH 5.5 was identified as the optimal operational pH for the nZVI@HNTs + H_2O_2 system.

According to previous studies, DO in the water is one of key factors affecting the degradation behavior of nZVI and Fenton reaction [53]. Therefore, to explore the influence of DO on the performance of nZVI@HNTs + H_2O_2 system, the TC solution was oxygenated or deoxygenated by bubbling air or high-purity N_2 for 30 min prior to adding nZVI@HNTs, and aeration was continued during the reaction. The reaction in air was treated as the blank experiment. Blank experiment, bubbling air, and bubbling N_2 stand for low DO concentration, high DO concentration, and no DO, respectively. Only 56.09 % of the TC was removed when air was bubbled, indicating that the removal efficiency of TC was significantly inhibited in air (Fig. 2g). This is because that the DO can passivate nZVI, which limit the release of Fe^{2+} and the generation of ROS [54]. Nevertheless, nZVI@HNTs + H_2O_2 system exhibited a good performance in both blank group and anaerobic condition. In the stage 1, the removal efficiency of TC in anaerobic condition (52.63 %) was slightly

higher than that in blank group (47.10 %). This suggests that nZVI is very sensitive to DO, a small amount of DO also inhibits the redox process of nZVI. As the reaction proceeds to the stage 2, the removal efficiency of TC in blank group quickly increased to 82.74 %. This is because the existence of a small amount of DO is conducive to the activation of Fenton-like reaction.

Typical wastewater contains dissolved inorganic anions, such as NO_3^-, SO_4^{2-}, PO_4^{3-}, CO_3^{2-}, and Cl^- , which may interfere with the removal efficiency of TC. The effect of inorganic anions on the TC degradation was investigated at the concentration of 10 mmol/L (Fig. 2h). The order of influence on TC degradation was PO_4^{3-} > CO_3^{2-} > NO_3^- > SO_4^{2-} > Cl^-. PO_4^{3-} and CO_3^{2-} had a stronger effect on the TC removal efficiency than other anions, likely because they can form complexes with Fe^{2+}, adsorb on the surface of nZVI, and/or can quench ROS [18,55]. Addition of NO_3^-, SO_4^{2-}, and Cl^- also inhibited TC removal efficiency, decreasing it from 86.61 % to 70.06 %, 74.06 %, and 75.00 %, respectively. NO_3^- may be directly reduced by nZVI, which form competitive reactions with TC [56]. Both SO_4^{2-}, and Cl^- had a scavenger effect of ROS [57].

To assess the impact of loading nZVI into the lumen of HNTs on its utilization efficiency, the degradation efficiencies of TC by nZVI@HNTs, nZVI/HNTs, and nZVI + HNTs (physical mixture) were compared. The loading amount of nZVI in nZVI/HNTs was adjusted to match that in nZVI@HNTs (8.43 %, Table S3). XRD confirmed that both nZVI/HNTs and nZVI consisted of pure Fe^0 phases without impurities (Fig. S11 in Supporting information). In nZVI/HNTs, irregularly shaped nZVI particles were dispersed on the outer surface of HNTs (Figs. S12a and c in Supporting information), whereas pure nZVI consisted of small, agglomerated particles with a diameter of about 50 nm (Figs. S12b and d in Supporting information). Without the addition of H_2O_2, the degradation efficiency of TC followed the order: nZVI/HNTs (80.74 %) > nZVI + HNTs (79.05 %) > nZVI@HNTs (67.1 %) (Fig. S13 in Supporting information). This difference can be attributed to the slower diffusion and reduced contact between nZVI and TC in nZVI@HNTs due to the encapsulation by HNTs, whereas nZVI and nZVI/HNTs provided more exposed active sites facilitating better interaction with TC. However, in the nZVI-Fenton system, the degradation efficiency of TC by nZVI@HNTs + H_2O_2 was 1.93 % and 3.71 % higher than those of nZVI/HNTs + H_2O_2 and nZVI + HNTs + H_2O_2, respectively, within 90 min. This improvement was primarily seen in stage 2, where the degradation rate constant k_2 of nZVI@HNTs (0.2240 min^{-1}) was significantly higher compared to nZVI/HNTs (0.1079 min^{-1}) and nZVI + HNTs (0.1248 min^{-1}) (Fig. S14 in Supporting information). The superior ability of nZVI@HNTs to activate H_2O_2 is closely related to the loading position of nZVI within the HNTs, which protects nZVI from side reactions with H_2O_2 that would otherwise consume H_2O_2 without generating ROS.

High stability and reusability are critical for cost reduction and enhancing economic efficiency in practical applications. The cycle life of the catalysts was evaluated through successive experiments where the catalysts were separated by centrifugation, washed with ethanol, dried under vacuum at 60 °C, and reused for subsequent cycles. The degradation performance after five consecutive cycles highlighted the advantages of nZVI@HNTs (Fig. 2i). While the degradation efficiency of TC by nZVI/HNTs + H_2O_2 and nZVI + HNTs + H_2O_2 dropped significantly to 35.57 % and 49.84 %, respectively, after five cycles, nZVI@HNTs + H_2O_2 maintained a degradation efficiency of 64.03 %. This resilience can be attributed to the protective effect of HNTs and the controlled release of H_2O_2, which minimized the consumption of nZVI by substances other than TC over multiple cycles.

In order to compare the degradation behavior of nZVI@HNTs and nZVI/HNTs, the influence of environmental factors on TC degradation by nZVI/HNTs + H_2O_2 system were investigated. The variation of TC degradation increased by the catalyst dose and

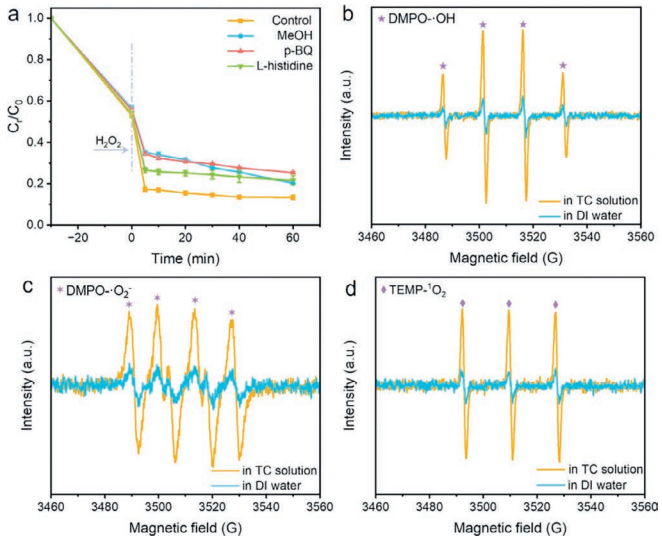


Fig. 3. (a) Effect of free radical scavengers on TC degradation by the nZVI@HNTs/H_2O_2 system. EPR signals of (b) DMPO-·OH, (c) DMPO-·O_2^-, and (d) TEMP-$^1O_2$ generated by the nZVI@HNT/H_2O_2 system with or without a 20 mg/L TC solution.

H_2O_2 concentration is similar to that of nZVI@HNTs + H_2O_2 system (Figs. S15a and b in Supporting information). As opposed to nZVI@HNTs, the degradation efficiency in nZVI/HNTs + H_2O_2 system of 10 mg/L TC is higher than that of 20 mg/L TC (Fig. S15c in Supporting information). This was attributed to the different adsorption behavior when nZVI grows on the outer surface of HNTs. In addition, the adaptability of nZVI/HNTs to pH is better, and the degradation efficiency of TC is 48.62 % at pH 11 (Fig. S15d in Supporting information). Interestingly, both anaerobic and aerobic conditions significantly inhibited the TC degradation by degradation (Fig. S15e in Supporting information). The effect of inorganic anions on the TC degradation by nZVI/HNTs + H_2O_2 system was consistent with that by nZVI@HNTs + H_2O_2 system (Fig. S15f in Supporting information).

To understand the role of ROS in the degradation system, radical quenching experiments and ESR analysis were performed. MeOH, p-BQ, and L-histidine were used as scavengers for ·OH, ·O_2^-, and $^1O_2$, respectively. As depicted in Fig. 3a, the addition of MeOH, p-BQ, and L-histidine reduced the degradation efficiency of TC from 86.62 % to 79.84 %, 74.64 %, and 78.39 %, respectively. This indicates the involvement of both radical and nonradical pathways in the degradation process [58]. Notably, MeOH and p-BQ exhibited stronger inhibition compared to L-histidine during stage 2, highlighting the crucial roles of ·OH and ·O_2^- in the rapid degradation facilitated by the nZVI-Fenton process. In the ESR experiments (Figs. 3b and c), 5,5-dimethylpyrroline-*N*-oxide (DMPO) was used to trap ·OH and ·O_2^-, while 4-amino-2,2,6,6-tetramethylpiperidine (TEMP) was used to trap $^1O_2$ (Fig. 3d). The spectra revealed signals corresponding to DMPO-·OH (1:2:2:1 signal intensity), DMPO-·O_2^- (1:1:1:1 signal intensity), and TEMP-$^1O_2$ (1:1:1 triplet signal intensity), confirming the presence of ·OH, ·O_2^-, and $^1O_2$ during the degradation process [59,60]. Interestingly, ESR analysis of the nZVI-Fenton process in the absence of pollutants showed lower intensities of DMPO-·OH, DMPO-·O_2^-, and TEMP-$^1O_2$ signals. This suggests that the interaction between nZVI@HNTs and TC enhances ROS generation by releasing more Fe^{2+} to activate H_2O_2. However, nZVI@HNTs may also undergo unexpected side reactions with H_2O, O_2, and other species, influencing the overall reaction kinetics.

To study the ability of combined nZVI-Fenton technology to promote mineralization, the changes in total organic carbon (TOC) content in the nZVI@HNT and nZVI@HNT + H_2O_2 systems were

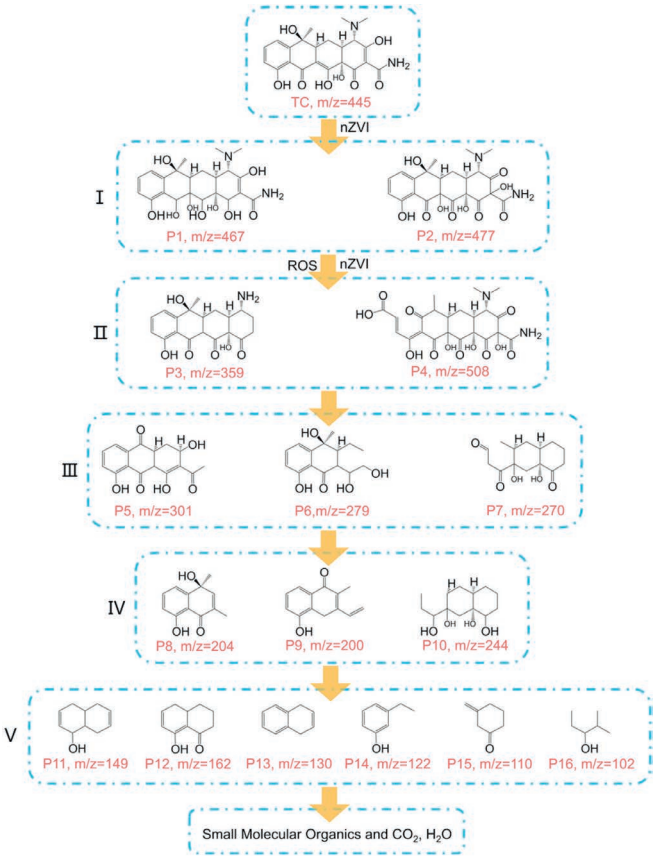


Fig. 4. Proposed degradation pathway of TC and the chemical structure of the intermediates.

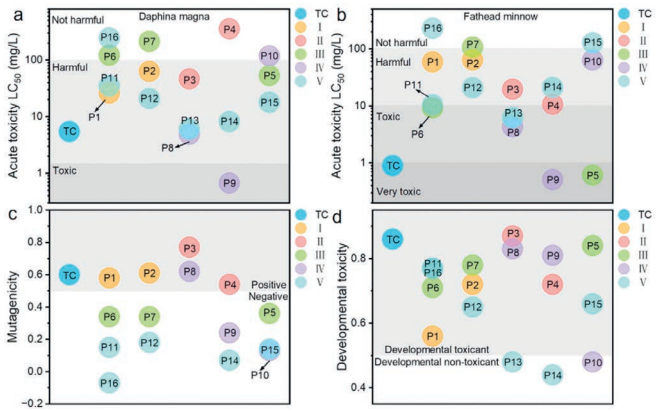


Fig. 5. (a) Acute toxicity of daphnia magna LC_{50}-48 h, (b) acute toxicity of fathead minnow LC_{50}-96 h, (c) mutagenicity, and (d) developmental toxicity of TC and its intermediates.

compared (Fig. S16 in Supporting information). The removal efficiency of TOC in the nZVI@HNTs + H_2O_2 system (6.26 %) was about 3 times greater than that in the nZVI@HNTs system (1.99 %). To enhance the removal efficiency of TOC through the nZVI-Fenton process, it is essential to note that complete mineralization of TC may not occur, resulting in the formation of intermediates. LC-MS analysis was employed to identify these intermediates in the nZVI@HNTs + H_2O_2 system, generating total ion chromatograms at various reaction times (Fig. S17 in Supporting information). Mass spectra at specific retention times (0.95, 1.23, 4.5, 5.48, 6.85, 8.23, and 12.5 min) were analyzed (Fig. S18 in Supporting information), proposing potential molecular structures and outlining a plausible degradation pathway (Fig. 4). Initially, TC undergoes preferential opening of double bonds facilitated by nZVI, followed by possible hydrogenation and hydroxylation of C=O, transforming into intermediates P1 and P2 [61,62]. Subsequent steps involve *N*-demethylation, deacetamido reactions forming intermediate P3, and dehydration leading P2 to convert into P4, disrupting polycyclic structures [63]. Further reactions include deamination, naphthalene ring cleavage, and hydroxyl radical rearrangements, yielding intermediates P5, P6, and P7 [64,65]. Reduction *via* demethylation, carbonylation, and dehydroxylation results in formation of P8, P9, and P10, followed by further opening of ring structures generating P11, P12, P13, P14, P15, and P16 [66,67]. Ultimately, these small molecule intermediates may fragment into CO_2 and H_2O, contributing to the partial mineralization process. This comprehensive analysis elucidates the transformation pathway of TC under nZVI@HNTs + H_2O_2 treatment, highlighting the formation of various intermediate species and their potential contribution to overall degradation mechanisms.

Based on the results from TOC and LC-MS analyses, some intermediates remain in the solution post-degradation. Hence, QSAR predictions using T.E.S.T. software were employed to evaluate TC and its intermediates for four key factors: 50 % Lethal Concentration (LC_{50}) of acute toxicity to Daphnia magna for 48 h (LC_{50}-48 h), acute toxicity to fathead minnow (LC_{50}-96 h), mutagenicity, and developmental toxicity [68]. The LC_{50}-48 h value of TC for Daphnia magna was found to be 5.44 mg/L, indicating it is harmful (Fig. 5a). Most intermediates showed lower acute toxicity to Daphnia magna compared to TC, except for P8 (0.67 mg/L) and P9 (4.89 mg/L). Notably, P4 (357.01 mg/L), P6 (121.72 mg/L), P7 (213.74 mg/L), P10 (118.86 mg/L), and P16 (245.43 mg/L) were classified as non-harmful to Daphnia magna. Regarding acute toxicity to fathead minnows (Fig. 5b), while P5 (0.61 mg/L) and P9 (0.51 mg/L) were highly toxic, most other intermediates exhibited reduced toxicity compared to TC, suggesting a transformation to less toxic forms by the nZVI@HNTs + H_2O_2 system. In terms of mutagenicity (Fig. 5c), TC and early-stage intermediates (I and II) showed positive mutagenicity (>0.5). However, as degradation proceeded, almost all subsequent intermediates displayed negative mutagenicity (<0.5). Additionally, developmental toxicity assessments revealed that most intermediates, except P3, had lower developmental toxicity compared to TC (Fig. 5d). Notably, P10 (0.48), P13 (0.48), and P14 (0.44) were classified as non-toxicants in terms of developmental toxicity. In summary, the nZVI@HNTs + H_2O_2 system effectively reduces the overall toxicity of TC by converting it into intermediates with generally lower acute toxicity, mutagenicity, and developmental toxicity. This underscores its potential as a practical approach to mitigate the environmental impact of TC contamination.

In conclusion, nZVI was successfully confined inside the lumen of HNTs by vacuum loading and heat-reduction treatment. The “protective function” mechanism of HNTs in nZVI@HNTs system primarily stems from spatial isolation and confinement effects. As carriers, HNTs act as barriers between nZVI and nontarget pollutants in the nZVI-Fenton process. Before H_2O_2 was added, the HNTs concentrated TC in the lumen by adsorption, reducing the possibility of a reaction between nZVI and H_2O. After introduction of H_2O_2, it cannot immediately contact nZVI because HNTs block diffusion, it preferentially interacts with the controlled-released Fe^{2+} from the nanoconfined space of HNTs to activate more ROS. The experimental results showed that the degradation efficiency of TC reached 86.61 % within 90 min ([TC] = 20 mg/L, initial pH 5.5, nZVI@HNTs dose = 0.5 g/L, and H_2O_2 concentration = 5.87 mmol/L). More importantly, this loading mode extends the sustained release of nZVI and enhances its stability. After 5 cycles, the degradation efficiency of nZVI@HNTs was more than twice that of nZVI/HNTs or nZVI + HNTs. In addition, TC was removed by the adsorption of HNTs, the strong reduction capacity of nZVI, and Fenton-like

reactions. In addition to active free radicals (·OH and $\cdot O_2^-$), active nonfree radicals ($^1O_2$) also play a key role. Moreover, TC is mainly transformed into small molecular organics by demethylation, ring opening, dihydroxylation, and hydroxyl radical rearrangement. Compared with those of TC, the acute toxicity, mutagenicity, and developmental toxicity of intermediates decreased with increasing degradation time. Research has shown that the nZVI@HNTs + H_2O_2 system is an efficient strategy for improving the utilization of nZVI and enhancing the degradation efficiency of organic pollutants.

CRediT authorship contribution statement

Yi Zhou: Writing – original draft, Investigation, Validation. **Guocheng Lv:** Conceptualization, Writing – review & editing, Funding acquisition. **Xinyu Lei:** Investigation, Visualization, Formal analysis. **Xinyu Hou:** Software. **Meng Liu:** Methodology. **Libing Liao:** Supervision. **Hailiang Dong:** Writing – review & editing, Supervision.

Acknowledgments

This work was financially supported by the National Natural Science Foundation of China (No. 42072053) and the National Key Research and Development Program of China (No. 2022YFC3702300).

Supplementary materials

Supplementary material associated with this article can be found, in the online version, at doi:10.1016/j.cclet.2025.111640.

References

[1] B.C. Hodges, E.L. Cates, J.H. Kim, Nat. Nanotechnol. 13 (2018) 642–650.
[2] T. Liu, S. Xiao, N. Li, et al., Nat. Commun. 14 (2023) 2881.
[3] A. Agrawal, P.G. Tratnyek, Environ. Sci. Technol. 30 (1996) 153–160.
[4] P. Huang, Z. Ye, W. Xie, et al., Water Res. 47 (2013) 4050–4058.
[5] M. Usman, J.M. Byrne, A. Chaudhary, et al., Chem. Rev. 118 (2018) 3251–3304.
[6] Y. Su, A.S. Adeleye, Y. Huang, et al., Water Res. 63 (2014) 102–111.
[7] J. Qu, Z. Li, F. Bi, et al., Proceed. Nat. Acad. Sci. U. S. A. 120 (2023) e2304552120.
[8] J. Xu, A. Avellan, H. Li, et al., Adv. Mater. 32 (2020) 1906910.
[9] X. Dong, Z. Chen, A. Tang, D.D. Dionysiou, H. Yang, Adv. Funct. Mater. 32 (2022) 2111565.
[10] X. Wang, J. Jing, M. Zhou, R. Dewil, Chin. Chem. Lett. 34 (2023) 107621.
[11] W.X. Zhang, C.B. Wang, H.L. Lien, Catal. Today 40 (1998) 387–395.
[12] G.H. Qasim, H. Fareed, M. Lee, W. Lee, S. Han, J. Hazardous Mater. 435 (2022) 128990.
[13] D. Meyerstein, Nat. Rev. Chem. 5 (2021) 595–597.
[14] C. Zhang, N. Ding, Y. Pan, L. Fu, Y. Zhang, Chin. Chem. Lett. 35 (2024) 109579.
[15] B. Li, J. Zhu, Chem. Engin. J. 255 (2014) 225–232.
[16] J. Deng, H. Dong, C. Zhang, et al., Separation Purif. Technol. 202 (2018) 130–137.
[17] Z. Diao, W. Chu, Sci. Total Environ. 754 (2021) 142155.
[18] Y. Chen, M. Zhang, T. Chen, et al., Appl. Catal. B: Environ. 324 (2023) 122270.
[19] L. Gong, L. Zhang, Chem. Commun. 59 (2023) 2081–2089.
[20] J. Lu, Q. Lu, L. Di, Y. Zhou, Y. Zhou, Chin. Chem. Lett. 34 (2023) 108357.
[21] I. Hussain, M. Li, Y. Zhang, et al., Chem. Engin. J. 311 (2017) 163–172.
[22] L. Santos-Juanes, F.S. García Einschlag, A.M. Amat, A. Arques, Chem. Engin. J. 310 (2017) 484–490.
[23] J. Fan, Y. Hu, X. Li, A.C.S. Sustain, Chem. Engin. 6 (2018) 15135–15142.
[24] S. Li, J. Tang, Q. Liu, X. Liu, B. Gao, Environ. Int. 138 (2020) 105639.
[25] X. Zhang, J. Tang, L. Wang, et al., Nat. Commun. 15 (2024) 917.
[26] C. Meng, B. Ding, S. Zhang, et al., Nat. Commun. 13 (2022) 4010.
[27] Y. Wang, Q. Zhao, Y. Guo, et al., Water Res. 264 (2024) 122220.
[28] Z. Yang, J. Qian, A. Yu, B. Pan, Proceed. Nat. Acad. Sci. 116 (2019) 6659–6664.
[29] A. Glotov, A. Vutolkina, A. Pimerzin, V. Vinokurov, Y. Lvov, Chem. Soc. Rev. 50 (2021) 9240–9277.
[30] P. Yuan, D. Tan, F. Annabi-Bergaya, Appl. Clay Sci. 112-113 (2015) 75–93.
[31] Y. Feng, X. Chen, R.R. He, et al., ACS Nano 18 (2024) 20001–20026.
[32] X.L. Duan, C.G. Yuan, K.Q. He, et al., Environ. Sci. Technol. 56 (2022) 4507–4517.
[33] P. Zhao, Y. Feng, Y. Zhou, C. Tan, M. Liu, Bioactive Mater. 20 (2023) 355-367.
[34] G.K. Dedzo, G. Ngnie, C. Detellier, ACS Appl. Mater. Interfaces 8 (2016) 4862–4869.
[35] Y. Feng, D. Zhang, X. Chen, C. Zhou, M. Liu, Adv. Funct. Mater. 34 (2024) 2307157.
[36] X. Jiang, A. Avellan, L. Hao, et al., Adv. Mater. 32 (2020) 1906910.
[37] H. Hamza, A.M. Ferretti, C. Innocenti, et al., Inorg. Chem. 59 (2020) 12086–12096.
[38] Q. Mao, Y. Zhou, Y. Yang, et al., J. Hazardous Mater. 380 (2019) 120848.
[39] L. Zhang, Y. Zhu, Y. Shi, et al., Environ. Sci. Pollution Res. 30 (2023) 85822–85834.
[40] L. Tan, S. Lu, Z. Fang, W. Cheng, E.P. Tsang, Appl. Catal. B: Environ. 200 (2017) 200–210.
[41] K. Kamil, W. Stanisław, S. Daniele, et al., J. Colloid Interf. Sci. 586 (2021) 655–662.
[42] L. Lorenzo, C. Giuseppe, P. Pooria, M. Stefana, L. Giuseppe, J. Colloid Interf. Sci. 547 (2019) 361–369.
[43] K. Peng, P.F. Wan, H.J. Wang, et al., Appl. Clay Sci. 212 (2021) 106211.
[44] Y. Lvov, W. Wang, L. Zhang, R. Fakhrullin, Adv. Mate. 28 (2015) 1227.
[45] H. Hamoon, D.L. Oreste, C. Dominic, Nat. Commun. 14 (2023) 664.
[46] B. Huang, Z. Wu, X. Wang, et al., Environ. Sci. Technol. 57 (2023) 15667–15679.
[47] S. Zha, Y. Cheng, Y. Gao, et al., Chem. Engin. J. 255 (2014) 141–148.
[48] C. Lin, S. Hsu, Separation Purif. Technol. 203 (2018) 111–116.
[49] X. Zhang, Y.R. Li, M.R. Wu, et al., Bioresource Technol. 320 (2021) 124264.
[50] Q. Wei, H. Li, Y. Guo, et al., J. Alloys Compd. 946 (2023) 169309.
[51] V. Viviana, A. Elshad, L.Y. M, Z. Andre, et al., Biomacromolecules 11 (2010) 820–826.
[52] H.M. Ibrahim, M. Awad, A.S. Al-Farraj, A.M. AlTurki, Nanomaterials 10 (2020) 192.
[53] H. Dong, C. Zhang, J. Deng, Water Res. 135 (2018) 1–10.
[54] H. Cheng, C. Huang, P. Wang, Environ. Res. 227 (2023) 115752.
[55] T. Guo, L. Jiang, K. Wang, et al., Appl. Catal. B: Environ. 286 (2021) 119883.
[56] H. Zhou, S. Wu, Y. Zhou, et al., Environ. Int. 128 (2019) 77–88.
[57] Y. Sun, L. Xia, J. Wang, et al., Separation Purif. Technol. 330 (2024) 125238.
[58] S. Li, X. Liu, Y. Zheng, et al., Chin. Chem. Lett. 35 (2024) 108971.
[59] P. Xu, R. Wei, P. Wang, et al., Environ. Sci. Technol. 58 (2024) 17464–17474.
[60] S. Feng, T. Xie, J. Wang, et al., Chem. Engin. J. 470 (2023) 143900.
[61] J.A. Donadelli, B. Caram, M. Kalaboka, et al., J. Environ. Chem. Engin. 8 (2020) 103624.
[62] Z.J. Xiao, X.C. Feng, H.T. Shi, et al., J. Hazardous Mater. 424 (2022) 127247.
[63] X. Wang, J. Tong, J. Ma, Reactive Funct, Polym 192 (2023) 105704.
[64] L. Tian, G. Lv, L. Wu, et al., Appl. Surf. Sci. 621 (2023) 156801.
[65] J. Zeng, W. Xie, Y. Guo, et al., Appl. Catal. B: Environ. 340 (2024) 123225.
[66] H. Dong, Z. Jiang, C. Zhang, et al., J. Colloid Interf. Sci. 513 (2018) 117–125.
[67] Q. Chen, H. Zhou, J. Wang, J. Bi, F. Dong, Appl. Catal. B: Environ. Energy 307 (2022) 121182.
[68] S. Xin, S. Huo, C. Zhang, et al., Appl. Catal. B: Environ. 305 (2022) 121024.